

Bidirectional sorting of flocking particles in the presence of asymmetric barriers

Jeffrey A. Drocco, C. J. Olson Reichhardt, and C. Reichhardt

Center for Nonlinear Studies and Theoretical Division,
Los Alamos National Laboratory, Los Alamos, NM 87545

(Dated: October 15, 2018)

We numerically demonstrate bidirectional sorting of flocking particles interacting with an array of asymmetric barriers. Each particle aligns with the average swimming direction of its neighbors according to the Vicsek model and experiences additional steric interactions as well as repulsion from the fixed barriers. We show that particles preferentially localize to one side of the barrier array over time, and that the direction of this rectification can be reversed by adjusting the particle-particle exclusion radius or the noise term in the equations of motion. These results provide a conceptual basis for isolation and sorting of single- and multi-cellular organisms which move collectively according to flocking-type interaction rules.

PACS numbers: 87.10.-e, 05.65.+b, 87.17.Jj, 05.40.-a

I. INTRODUCTION

The ensemble dynamics of self-driven particles can differ significantly from those of Brownian random walkers¹. For example, in experiments on microfabricated habitats connected by funnel-shaped channels, self-propelled *E. coli* bacteria preferentially migrated to the chamber towards which the funnels pointed^{2,3} even though Brownian particles would have remained equally distributed in both chambers. A simple simulation model showed that the rectification arises due to the modification of the run-and-tumble swimming dynamics of the bacteria by the walls of the microenvironment⁴. When a running bacterium encounters a wall, it does not reflect away from the wall or immediately tumble, but swims in the direction of the wall while preserving as much as possible its prior direction of motion. Refs.⁴ and⁵ found rectification under this interaction rule for independent swimmers that did not interact with each other. The rectification in the bacteria system resembles a ratchet effect in which a net dc motion occurs in the absence of a dc drive due to the application of an external ac drive or flashing substrate⁶. For self-driven particles, however, no external driving is necessary. In addition to demonstrations of directed bacterial motion achieved through a ratchet mechanism⁷, it has also been shown that baths of swimming bacteria can induce directed rotational motion of asymmetric flywheels^{8–10}.

Interactions between self-propelled particles can lead to distinctive dynamical behaviors that are more complex than those of independently moving particles. Simple models such as that of Vicsek *et al.*^{11,12} capture many features of the dynamics of species with strongly collective motion, in which individuals preferentially align with their neighbors and form moving groups^{13,14}. These models qualitatively reproduce the motion of both macro-scale groups, such as fish schools and bird flocks^{15,16}, and micro-scale groups, such as bacterial swarms and cancerous tumors¹⁷. The original Vicsek model includes only a term for preferential velocity alignment with all neighbors within a fixed flocking radius,

yet it exhibits a phase transition to unidirectional motion as a function of particle density and noise amplitude. Although numerous modifications of the Vicsek model have been proposed, such as the addition steric interactions¹⁸ and/or cohesion^{19–21}, only a very limited amount of work has been done on the interaction of flocking particles with walls or barriers. Walls can impose a directional symmetry breaking¹⁴, induce the formation of a vortex state^{18,22–24} or laning²⁵, or simply serve as aggregation focal points²⁶; walls have also been used for understanding finite size effects^{27–29}, such as the relationship between the collective dynamics of fish in a tank and those of fish in the open ocean.

In this work we simulate a modified version of the Vicsek flocking algorithm that includes both steric repulsion between particles and confinement within a two-dimensional microenvironment with strategically placed gates similar to those of Ref.⁴. Here we consider strictly repulsive particle-wall interactions, so that the particles do not follow the walls when swimming independently. As the particle density increases, we find rectification effects once the density is high enough to permit collective motion to occur. By varying the interparticle exclusion radius, the flocking radius, or the noise, we can reverse the direction of the rectification. This result has implications for the potential sorting of self-propelled particles that move according to these types of interaction rules.

Simulation—We consider a two-dimensional $L \times L$ system of N self-driven particles at number density $\rho_0 = N/L^2$ with fixed, repulsive boundaries on all sides. The overdamped equation of motion for a single particle i is $d\mathbf{x}_i = \mathbf{v}_i(t)dt$ with

$$\mathbf{v}_i(t) = \mathbf{f}_{vc}^i(t) + \mathbf{f}_r^i(t) + \mathbf{f}_b^i(t) \quad (1)$$

All quantities are rescaled to dimensionless units. The time step $dt = 0.002$ and we take $L = 66$. The velocity consensus force \mathbf{f}_{vc}^i , also called the alignment force, is determined by the velocities of all M particles, including particle i , within a flocking radius r_f of particle i :

$$\mathbf{f}_{vc}^i(t) = A_f (\cos(\Phi_{vc}^i(t))\hat{\mathbf{x}} + \sin(\Phi_{vc}^i(t))\hat{\mathbf{y}}) \quad (2)$$

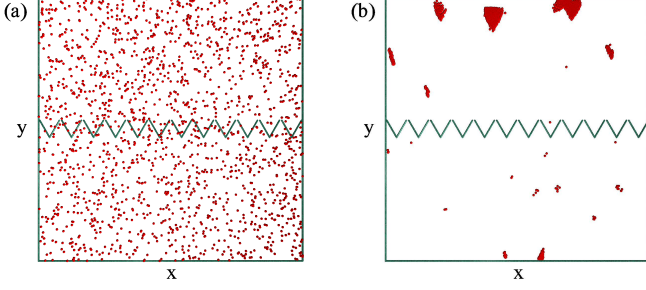


Figure 1: Simulation images. Lines: barriers and walls; dots: particle positions. a) Initial state of sample with $r_f = 1.0$ and $r_e = 0.07$ at $\rho_0 = 0.4$. b) The same sample after 7×10^5 simulation time steps shows rectification of particles into the top chamber.

with

$$\Phi_{vc}^i(t) = \arctan^2 \left(\sum_{j=1}^M \frac{\mathbf{v}_j(t-dt)}{|\mathbf{v}_j(t-dt)|} \right) + \xi. \quad (3)$$

Here $A_f = 2.0$ and ξ is a random variable uniformly distributed on the interval $[-\eta/2, \eta/2]$. Both the steric particle-particle interactions \mathbf{f}_r^i and the particle-barrier interactions \mathbf{f}_b^i are given by the stiff spring repulsions: $\mathbf{f}_r^i(t) = \sum_{j \neq i}^N A_r (2r_e - r_{ij}) \Theta(2r_e - r_{ij}) \hat{\mathbf{r}}_{ij}$ and $\mathbf{f}_b^i(t) = \sum_k^{N_g} A_p (r_e + r_g - r_{ik}) \Theta(r_e + r_g - r_{ik}) \hat{\mathbf{r}}_{ik}$, where $A_r = 200$, $A_p = 10$, $r_{ij} = |\mathbf{r}_i(t) - \mathbf{r}_j(t)|$, and $\hat{\mathbf{r}}_{ij} = [\mathbf{r}_i(t) - \mathbf{r}_j(t)]/r_{ij}$. Here r_e is the particle exclusion radius, $r_g = 0.05$ is the barrier exclusion radius, and there are $N_g = 16$ barriers composed of the four confining walls plus 12 V-shaped gates. \mathbf{r}_{ik} is the vector from the nearest point on barrier k to particle i , $r_{ik} = |\mathbf{r}_{ik}|$, and $\hat{\mathbf{r}}_{ik} = \mathbf{r}_{ik}/r_{ik}$. The length of each side of the V gates is $L_B = 4.9$ and the angle each V arm makes with the y axis is 30° . The spacing between the bases of the V's is $l_s = 5.5$ and the spacing between the tips of adjacent V's is $l_o = 0.6$. The 12 gates bisect the system into top and bottom chambers, with the aperture of each funnel shape pointing toward the top chamber. We initialize the system by distributing the particles at random throughout the sample. The equations of motion are then integrated for 3×10^6 simulation time steps. In the absence of particle-particle interactions, the purely repulsive wall interactions produce no rectification of the particles, in agreement with the results of Ref.⁵

Results— In Fig. 1(a), we show an image of the simulation geometry in the randomly initialized state for a system with $r_f = 1.0$, $r_e = 0.07$, and $\rho_0 = 0.4$. After a sufficient amount of time elapses, the particles concentrate in one of the two chambers, reaching a steady state value of ρ_{top} , the density in the top chamber. In Fig. 1(b), after 7×10^5 simulation time steps the particle density is clearly higher in the top chamber.

We find that we can vary whether the rectification moves the particles into the top ($\rho_{top} > \rho_0$) or bottom

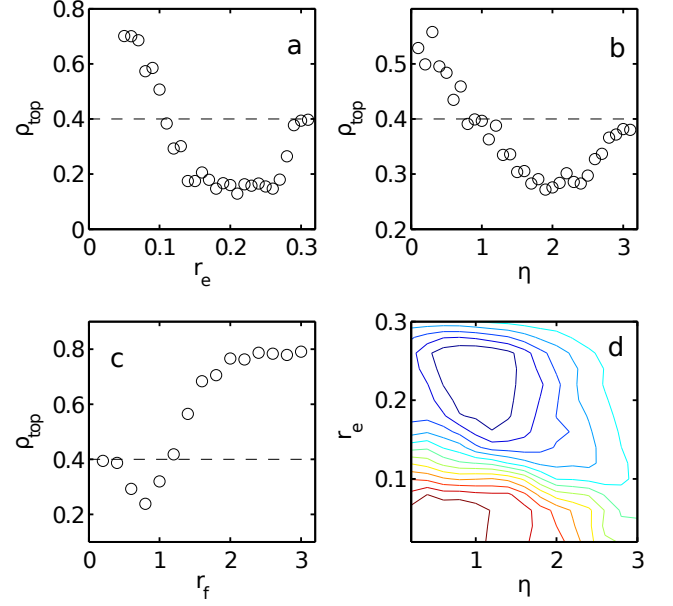


Figure 2: (a-c) ρ_{top} , the density in the top chamber, after 3×10^6 simulation time steps for a sample with initial density $\rho_0 = 0.4$, indicated by the dashed line. (a) ρ_{top} vs r_e for $\eta = 1.5$ and $r_f = 1.0$. The rectification reverses at $r_e = 0.12$ and drops to zero for $r_e \geq 0.3$. (b) ρ_{top} vs η for $r_e = 0.12$ and $r_f = 1.0$. The rectification reverses at $\eta \sim 1.0$ and drops to zero for $\eta \gtrsim \pi$. (c) ρ_{top} vs r_f for $r_e = 0.12$ and $\eta = 1.5$. For $r_f < r_e$ only steric particle interactions occur and rectification is negligible. There is a rectification reversal at $r_f \approx 1.2$, and for large r_f when all the particles tend to align into a giant flock, the particles accumulate in the top chamber. (d) Rectification phase diagram for r_e vs η . Lower contours (red) indicate rectification into the top chamber and upper contours (blue) indicate rectification to the bottom chamber.

($\rho_{top} < \rho_0$) chamber by altering r_f , r_e , or η , as shown in Fig. 2(a-c) where we plot ρ_{top} after 3×10^6 simulation time steps. For small values of r_e and η , particles are rectified into the top chamber, but a rectification reversal occurs at $r_e = 0.12$ and $\eta \sim 1.0$ in Fig. 2(a) and (b), respectively. There is a saturation into a nonrectifying state for $r_e \geq 0.3$ in Fig. 2(a); this corresponds to $2r_e \geq l_o$ and occurs when the particle diameter becomes larger than the aperture between adjacent gates, so that particles can no longer pass between the upper and lower chambers. In Fig. 2(b) rectification vanishes for $\eta \gtrsim \pi$ when the alignment force between neighboring particles, and thus the tendency of particles to form flocks, is almost completely destroyed by noise. We plot a rectification phase diagram as a function of r_e and η in Fig. 2(d), showing that rectification into the upper chamber occurs for small values of r_e and η , while reversed rectification into the lower chamber appears for larger r_e and small η .

We next consider the flocking radius r_f . Fig. 2(c) indicates that no rectification occurs when $r_f < r_e$. In this limit, the particles interact only sterically and have

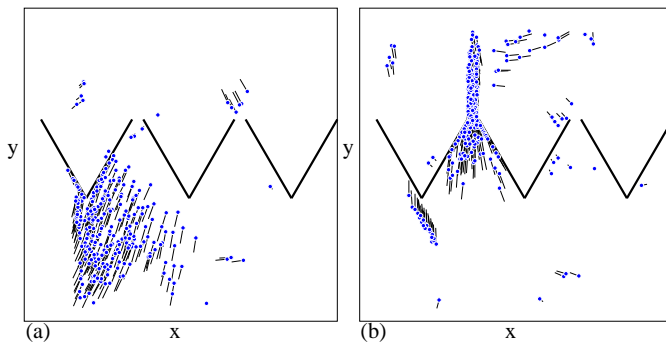


Figure 3: Illustration of rectification into the top chamber for low noise $\eta = 1.5$ and small exclusion radius $r_e = 0.05$ at $r_f = 1.0$. A 15×15 section of the sample is shown. Dots: particle positions; light lines: particle trajectories; heavy lines: barriers. A flock incident on the gates from the bottom chamber (a) condenses and elongates in order to file through the aperture between gates (b). Flocks incident on the gates from the top chamber have a much lower probability of passing through the aperture and cannot be funneled into a similar oblong shape.

no flocking interaction, and the repulsive barrier walls produce no rectification in the absence of flocking. For $r_e < r_f < 1.2$, we find a reversed rectification into the lower chamber, while for all $r_f \geq 1.2$, the particles rectify into the top chamber. For $r_f > 2.0$, the value of ρ_{top} saturates at $\rho_{top} = 0.8 = 2\rho_0$, indicating that nearly all of the particles are located in the top chamber.

The rectification reversal occurs due to a change in the nature of the microscopic interaction between the flocks and the funnel channels. For example, as the exclusion radius r_e increases, the particles are less able to form tight and cohesive flocks. At low values of r_e , particles are rectified into the top chamber when flocks, incident on the gates from the bottom, rearrange into oblong shapes and pass efficiently through the funnel, as illustrated in Fig. 3. For higher values of r_e , the steric interparticle repulsion prevents the flocks from condensing and makes it impossible for more than one particle at a time to pass through the funnel aperture. As a result, the particles clog inside the funnel rather than passing through, as illustrated in Fig. 4(a). The flock reverses direction due to the repulsion from the barrier walls, and at most one or two particles occasionally manage to escape the flock and enter the top chamber, as shown in Fig. 4(b). In contrast, a flock that approaches the gates from the upper chamber is fragmented by the gates into two smaller flocks; when this occurs, particles that are directly incident on the aperture between gates can escape from both flocks and pass in a single file into the lower chamber, as illustrated in Fig. 4(c,d,e). Since the average number of particles escaping the flock and crossing the barrier is larger when the flocks are approaching from above than when they are approaching from below, a net rectification into the lower chamber occurs over time. We note that the reversed rectification into the lower chamber (Fig. 4)

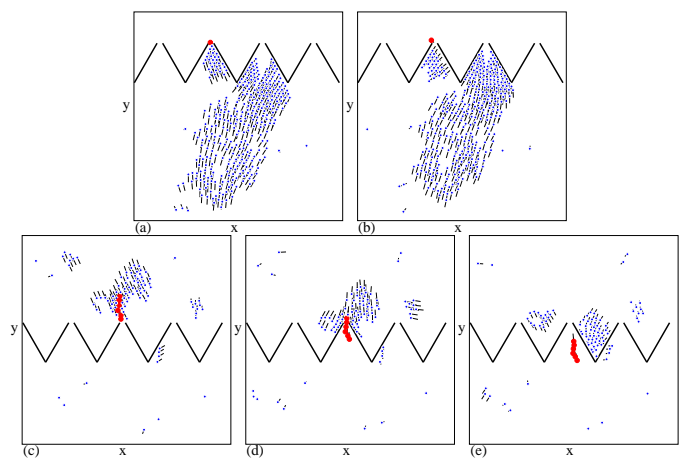


Figure 4: Illustration of rectification into the lower chamber for low noise $\eta = 1.5$ and large exclusion radius $r_e = 0.2$ at $r_f = 1.0$. A 20×20 section of the sample is shown. Dots: particle positions; light lines: particle trajectories; heavy lines: barriers. (a,b) Flocks incident on gates from the bottom chamber cannot fit through the aperture for this value of r_e ; the flock jams inside the funnel while a single particle (highlighted in red) escapes from the flock and enters the upper chamber. The remainder of the flock returns to the lower chamber. (c,d,e) Flocks incident on gates from the top chamber are fragmented and a small group of particles (highlighted in red) can escape from the flock and enter the lower chamber. The flock fragmentation process occurs with greater frequency as the flocks become less cohesive due to either higher η or higher ratios r_e/r_f .

is a much slower process than the forward rectification into the higher chamber (Fig. 3), although we are able to reach a steady state within our simulation time for either process. In spite of this, we find that the maximum possible amount of rectification that can be achieved in steady state as the parameters are varied is the same for both directions of rectification, as shown in Fig. 2(a).

Reversed rectification into the lower chamber also occurs whenever the flocks become fragile or prone to breakage. This occurs both when the noise parameter η is increased and when the flocking radius r_f is reduced. Under these conditions, the flocks are not cohesive enough to flow as a unit through the funnel aperture in the manner illustrated in Fig. 3; at the same time, the probability that a flock will fragment and lose some of its members to the lower chamber when approaching the gates from above, as in Fig. 4(c-e), is increased. In Fig. 5(a), we plot the average flock size N_c as a function of r_f , r_e , and η for the systems in Fig. 2. We separate the particles into clusters iteratively by identifying particles that are within the flocking radius r_f of each other; N_c is then the average number of particles per cluster. The value of N_c is higher in regimes where the particles are rectified to the top of the container, and lower in the reversed rectification regime.

One of the unique aspects of the rectification behavior

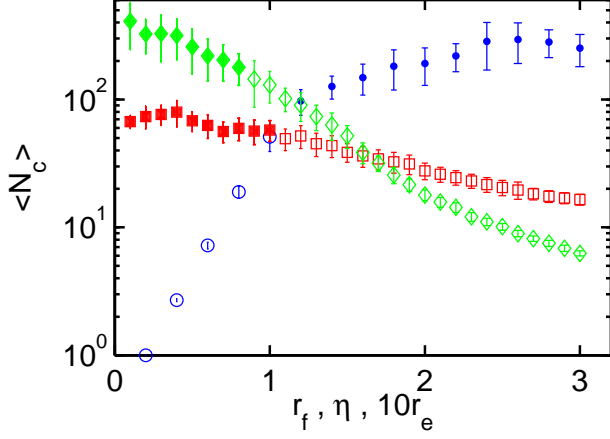


Figure 5: Mean flock size N_c , in number of particles, vs r_f (blue circles), r_e (red squares), and η (green diamonds). Error bars indicate standard deviation.

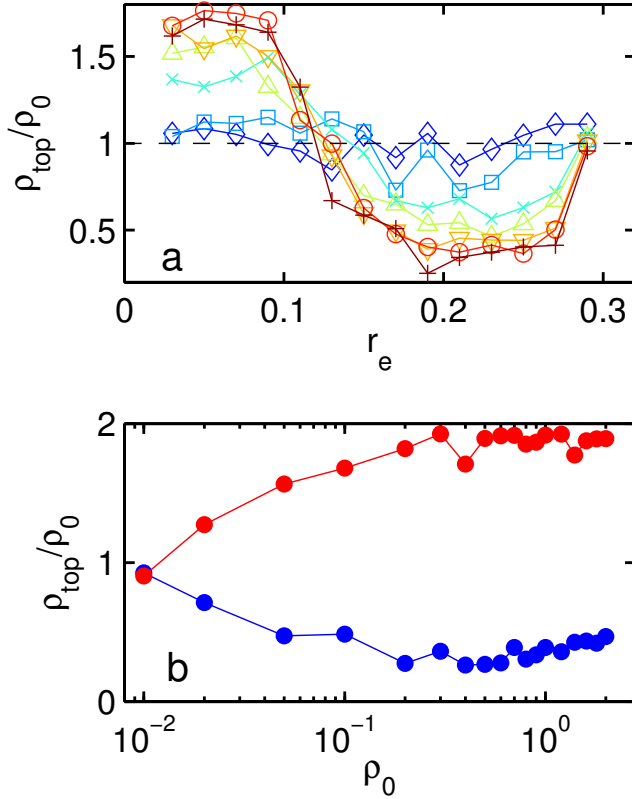


Figure 6: Dependence of rectification on initial particle density ρ_0 for a system with $r_f = 1.0$ and $\eta = 1.1$. (a) ρ_{top}/ρ_0 after 3×10^6 simulation time steps vs r_e for different values of ρ_0 . From blue to red, $\rho_0 = 0.004$ (\diamond), 0.01 (\square), 0.03 (\times), 0.05 (\triangle), 0.08 (∇), 0.1 (\circ), 0.12 ($+$). A rectification reversal emerges as ρ_0 increases. (b) ρ_{top}/ρ_0 after 3×10^6 time steps vs ρ_0 for $r_e = 0.05$ (upper red curve) and $r_e = 0.23$ (lower blue curve).

described here is that, unlike previous rectification phenomena reported for self-driven particles², it occurs only when the initial particle density ρ_0 is high enough for flock formation to occur. In the limit of low ρ_0 , when the particles are moving independently and not able to form flocks, individual particles simply reflect off the barriers in a manner similar to inertial particles. This type of barrier interaction has been shown to produce no rectification in noninteracting particle limit⁵, and as indicated in Fig. 6(a) we find no rectification at low densities $\rho_0 < 0.01$. As ρ_0 increases, both rectification and a rectification reversal emerge, and the amount of rectification saturates for $\rho_0 \geq 0.1$, as shown in Fig. 6(b). We note that since ρ_0 represents number density, rather than surface area covered, it is possible to have $\rho_0 > 1$.

Conclusion— We have implemented a simple model of flocking particles in the presence of fixed, repulsive barriers, and find that such particles will concentrate on one side of a set of asymmetric V-shaped gates. The direction of the rectification can be reversed by modulating any of three parameters: the flocking radius r_f , the exclusion radius r_e , or the noise parameter η . The existence of the rectification and its direction are determined by the ability of the particles to form flocks and the robustness of the flocks against breakage; in the low density limit, when no flocks appear, we find no rectification due to the purely repulsive interactions of the particles with the barrier walls. Thus, the rectification we observe arises strictly due to collective effects. The bi-directional rectification behavior we describe could be used to sort particles which tend to concentrate on different sides of the barrier³⁰. This effect is similar to the sorting phenomenon observed by Mahmud *et al.* for cancer cells³¹. We expect sorting devices based on these principles to have broad potential applications with regard to both biomedical diagnostics and therapeutics.

This work was carried out under the auspices of the NNSA of the U.S. DoE at LANL under Contract No. DE-AC52-06NA25396.

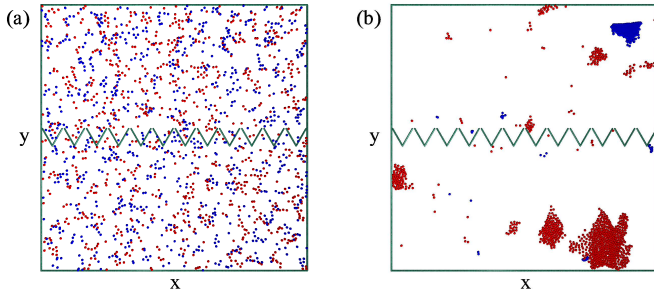


Figure 7: Supplemental Figure. Demonstration of two-species sorting. Simulation of system containing 871 "A" particles with $r_e = 0.22$ (green) and 871 "B" particles with $r_e = 0.055$ (pink). $r_f = 1.0$ and $\eta = 1.1$ in both cases. Particles of different species repel via steric repulsion but only experience alignment forces with particles of the same species. Simulation shown (a) at time $t = 0$ and (b) after 4×10^6 simulation time steps when many of the "A" particles have rectified into the bottom chamber and most of the "B" particles have rectified into the top chamber. The bidisperse system requires longer times to reach a steady state compared to the monodisperse system.

-
- ¹ B. ten Hagen, S. van Teeffele, and H. Löwen, J. Phys.: Condens. Mat. **23**, 194119 (2011).
 - ² P. Galajda, J. Keymer, P. Chaikin, and R. Austin, J. Bacteriol. **189**, 8704 (2007).
 - ³ P. Galajda, J. Keymer, J. Dalland, S. Park, S. Kou, and R. Austin, J. Mod. Optics **55**, 3413 (2008).
 - ⁴ M.B. Wan, C.J.O. Reichhardt, Z. Nussinov, and C. Reichhardt, Phys. Rev. Lett. **101**, 018102 (2008).
 - ⁵ J. Tailleur and M.E. Cates, EPL **86**, 60002 (2009).
 - ⁶ P. Reimann, Phys. Rep. **361**, 57 (2002).
 - ⁷ B. Kaehr and J.B. Shear, Lab Chip **9**, 2632 (2009).
 - ⁸ R. Di Leonardo *et al.*, Proc. Natl. Acad. Sci. (USA) **107**, 9541 (2010).
 - ⁹ A. Sokolov, M.M. Apodaca, B.A. Grzybowski, and I.S. Aranson, Proc. Natl. Acad. Sci. (USA) **107**, 969 (2010).
 - ¹⁰ L. Angelani, R. Di Leonardo, and G. Ruocco, Phys. Rev. Lett. **102**, 048104 (2009).
 - ¹¹ T. Vicsek, A. Czirók, E. Ben-Jacob, I. Cohen, and O. Shochet, Phys. Rev. Lett. **75**, 1226 (1995).
 - ¹² A. Czirók, H.E. Stanley, and T. Vicsek, J. Phys. A: Math. Gen. **30**, 1375 (1997).
 - ¹³ J. Toner, Y. Tu, Phys. Rev. Lett. **75**, 4326 (1995).
 - ¹⁴ J. Toner, Y. Tu, Phys. Rev. E **58**, 4828 (1998).
 - ¹⁵ D.J.T. Sumpter, Phil. Trans.: Biol. Sci. **361**, 5 (2006).
 - ¹⁶ I.D. Couzin, Trends Cognit. Sci. **13**, 36 (2009).
 - ¹⁷ T.S. Deisboeck and I.D. Couzin, Bioessays **31**, 190 (2009).
 - ¹⁸ A. Czirók, E. Ben-Jacob, I. Cohen, and T. Vicsek, Phys. Rev. E **54**, 1791 (1996).
 - ¹⁹ I.D. Couzin, J. Krause, R. James, G.D. Ruxton, and N.R. Franks, J. Theor. Biol. **218**, 1 (2002).
 - ²⁰ G. Grégoire and H. Chaté, Phys. Rev. Lett. **92**, 025702 (2004).
 - ²¹ M.R. D'Orsogna, Y.L. Chuang, A.L. Bertozzi, and L.S. Chayes, Phys. Rev. Lett. **96**, 104302 (2006).
 - ²² Y.L. Duparcmeur, H. Herrmann, and J.P. Troadec, J. Phys. I France **5**, 1119 (1995).
 - ²³ B. Szabó, G.J. Szöllösi, B. Gönci, Zs. Jurányi, D. Selmeczi, and T. Vicsek, Phys. Rev. E **74**, 061908 (2006).
 - ²⁴ A.B.T. Barbaro, K. Taylor, P.F. Trethewey, L. Youseff, and B. Birnir, Math. Comput. Sim. **79**, 3397 (2009).
 - ²⁵ J.P. Hernandez-Ortiz, P.T. Underhill, and M.D. Graham, J. Phys.: Condens. Matter **21**, 204107 (2009).
 - ²⁶ J.P. Hernandez-Ortiz, C.G. Stoltz, and M.D. Graham, Phys. Rev. Lett. **95**, 204501 (2005).
 - ²⁷ D.J. Hoare, I.D. Couzin, J.-G.J. Godin, and J. Krause, Animal Behav. **67**, 155 (2004).
 - ²⁸ E. Hensor, I.D. Couzin, R. James, and J. Krause, Oikos **110**, 344 (2005).
 - ²⁹ C.K. Hemelrijk, H. Hildenbrandt, J. Reinders, and E.J. Stamhuis, Ethology **116**, 1099 (2010).
 - ³⁰ See EPAPS Document xx.
 - ³¹ G. Mahmud *et al.*, Nature Phys. **5**, 606 (2009).